



A Planely Fundamental Survey

Based on a contribution solicited from Russell J. Smith (University of Waterloo)

The NOAO Fundamental Plane Survey (NFPS), initiated in 1999, is capitalizing on the wide-field imaging and spectroscopic capabilities at the KPNO and CTIO 4-m telescopes to investigate the structure, contents, and motions of nearby galaxy clusters. The NFPS is led by Mike Hudson (University of Waterloo). Collaborators are John Lucey, Stephen Moore, Stephen Quinney, and Roger Davies (University of Durham); Gary Wegner and Jenica Nelan (Dartmouth College); Nicholas Suntzeff (CTIO); David Schade (Canadian Astronomy Data Center); and Russell Smith.

The principal goal of the NFPS is to resolve the controversial issue of large-scale bulk flows in cluster samples, using the Fundamental Plane as a distance indicator relation. With ~50 early-type members observed per cluster, this method yields distances with random errors of <3%, allowing meaningful measurements of peculiar velocities out to distances in excess of $100 \text{ h}^{-1} \text{ Mpc}$. The award of NOAO survey time has allowed the NFPS continued access to stable instrumentation over the duration of the survey, a critical advantage given the importance of data homogeneity. In addition to their use for cosmic flows, the data will provide an unprecedented wealth of information on galaxy morphology and spectroscopic parameters for nearby cluster galaxies. For example, the survey will provide a firm low-redshift reference point for studies of cluster populations at moderate redshifts conducted on larger telescopes.

The sample consists of ~100 clusters within $z < 0.06$ distributed over the whole sky, selected by X-ray luminosity. Clusters have been imaged in the B and R bands, using the 8K Mosaic cameras at the CTIO Blanco 4-m, the KPNO Mayall 4-m, and the KPNO 0.9-m telescopes, with some extra data obtained from the CFHT 12K Mosaic, under the CHF queue program. B-R color-magnitude relations are then used to select red-sequence cluster members (i.e., likely early-type galaxies) for spectroscopic follow-up. The images will also be employed to measure morphological parameters (including bulge/disk decomposition) for all bright galaxies in the field. This computationally intensive task is being undertaken using a

high-performance “beowulf” cluster ($112 \times 667 \text{ MHz}$ alpha processors; see www.sharcnet.ca).

The spectroscopic program uses the Hydra multifiber spectrographs at the WIYN 3.5-m and Blanco 4-m telescopes. In each cluster, typically 40 to 70 galaxies (with $R < 17$ and “red” relative to the cluster color—magnitude relation) are observed, over the 60 arcmin or 40 arcmin field of view of the instruments. Spectral resolution and S/N are sufficient to measure redshifts, internal velocity dispersions, and a wide range of metal and Balmer-series absorption line indices over the spectral range 4000–6000 Å.

Early results from the spectroscopic observations will include a study of the line strength versus velocity dispersion relationships, and the possibility of environmental influences on these parameters. For example, it has long been known that the Mgb index at 5177 Å increases strongly with velocity dispersion, σ . This is likely due to a steady increase of metallicity with mass, as expected in galactic wind models

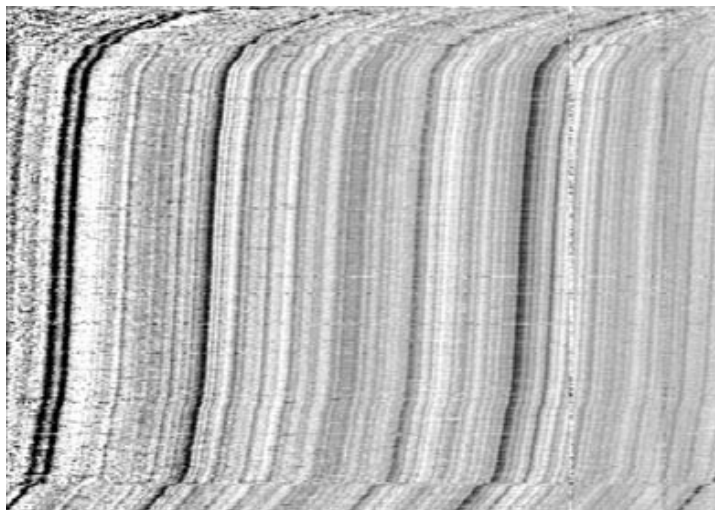


Figure 1. Galaxy spectra from a recent NFPS observing run. Each spectrum is plotted left to right from 3900 Å to 6100 Å, and stacked into the diagram in order of redshift, with the most distant (background) galaxies at the top. The strong Ca H+K doublet is seen at the left (blue), the G-band and Mgb features are prominent, while NaD is seen at the red end only for the nearest galaxies. The vertical noise feature results from sky subtraction residuals at 5577 Å. No restriction on signal-to-noise has been applied; a few spectra of poor data quality can be seen as the horizontal noise-streaks. These spectra, for ~900 galaxies, represent ~15% of the NFPS spectroscopic database.

continued



Planely Fundamental Survey continued

(although age can also influence this index). Interestingly, in some clusters *Mgb* is systematically stronger (at a given σ) for galaxies in the center of the cluster than for members further out. That is, galaxies near the cluster core may be more metal-rich, at given mass, than galaxies in the outskirts. An age interpretation (in the sense that outer members are younger) can be ruled out, due to the lack of any radial trend in residuals from the $H\gamma$ - σ relation.

This effect is found in NFPS data for a number of clusters so far (the case of Abell 3558 is shown here), and a similar effect has been noted for the Coma cluster in previous studies. However, initial indications are that such gradients are not ubiquitous in NFPS clusters. Since any existing cluster-centric gradient in metallicity (or indeed, in age) would probably be quickly erased by mixing in cluster mergers, it is possible that the presence of gradients might be correlated

with other indicators of “regularity” in clusters, such as cooling-flows, absence of substructure, etc.

As of July 2002, the survey’s imaging data are fully in hand and largely reduced, although morphological analysis is still under way. Spectroscopic data for most of the clusters has been obtained, with the more complex spectral reductions now in progress. In particular, a subset of clusters has been selected to serve as a testbed for many of the analyses foreseen, and data for these clusters is in an advanced stage. Efficient management and (useful) public release of the large quantity of data yielded by the survey present a significant challenge. An early release of image data can be found at the NFPS public Web page (astro.uwaterloo.ca/~mjhudson/nfjp). Ultimately, image data, spectra and parameter-rich catalogues will be made available via the NOAO science archive and/or via the CADC.

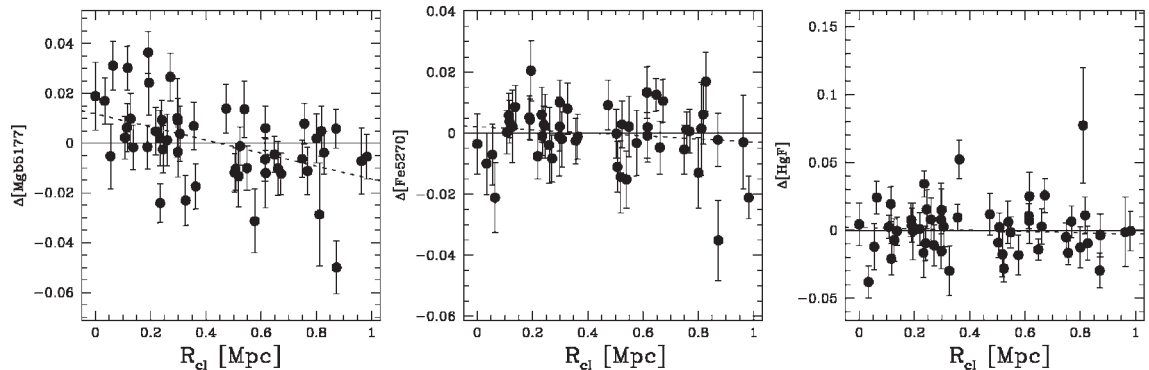


Figure 2. Residuals from the *Mgb*- σ , *Fe5270*- σ and $H\gamma$ -*Fe*, relations, plotted against cluster-centric distance R_{cl} , for galaxies in the rich cluster Abell 3558. Here the sample has been restricted to 55 galaxies with $\sigma > 160 \text{ km/s}^{-1}$, to exclude points with the largest error bars; the trends are formally unchanged if all ~ 90 galaxies are plotted. The significant $>3\sigma$ trend in the *Mgb* residuals suggests that centrally located galaxies have higher metallicity at a given mass than members further out. Note that the *Fe5270* line shows no strong trend (indeed, the four most central galaxies have lower Fe than expected for their mass). The lack of trend in $H\gamma$ Fe residuals strongly argues against an “age-gradient” interpretation.

A Wide-Field Survey for Stellar Variability

Based on a contribution solicited from Mark E. Everett & Steve B. Howell (Planetary Science Institute)

Mark Everett and Steve Howell used the Mosaic Camera at the KPNO 0.9-m as part of a high-precision variability study of Galactic field stars (PASP 113, 1428 and PASP 114, 656). Stellar variability at low amplitudes among solar type stars has not been studied extensively, yet represents a potential source of confusion for detecting extrasolar planets. The NASA Discovery mission Kepler, which aims to detect Earth-sized extrasolar planets transiting solar-type stars, will rely on the ability to

distinguish between transits and intrinsic stellar variability (at 0.1 millimagnitude levels). The Space Interferometry Mission (SIM) can expect at least some of its target stars (and possibly reference stars) to show astrometric variations due to spots and other asymmetries. Ground-based projects hoping to find transiting extrasolar planets must also distinguish between intrinsic stellar variations, grazing stellar eclipses, and true transits.

continued



Wide-Field Survey continued

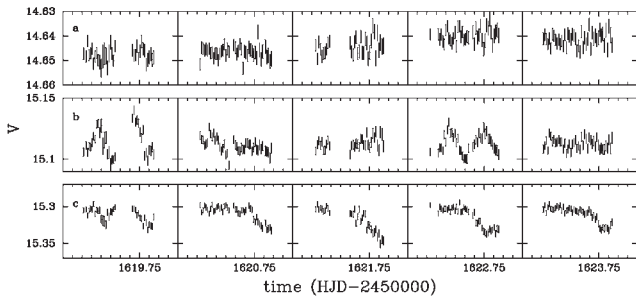


Figure 1. Light curves of three example variables. Each night of data is approximately 4.5 hours long. Panel (a) shows an unidentified class of variable. The colors and light curve suggest it may be a late-type spotted variable. Panel (b) shows a pulsating star, probably of the SX Phe class. Panel (c) shows an eclipsing variable.

The Everett and Howell study will identify signatures and frequency of intrinsic stellar variations and those spectral classes that are most variable or stable (which could serve as high-precision standards). Their survey is also useful for other stellar variability studies and should help define questions addressed by future projects like the Large Synoptic Survey Telescope (LSST), which will provide data for long-term stellar variability studies.

Time-series images were taken toward two 1-square degree fields on five consecutive nights in March 2000, sampling every 5 minutes to obtain light curves of all stars in the magnitude range $V = 14-19$. The data were reduced using automated procedures, including IRAF scripts, to produce light curves and UBVRI colors for each star in the field.

The light curves allow detection of millimagnitude amplitude variations in stars over a range of spectral types, as well as the quantification levels and frequency of variability in these populations. The data are particularly rich in G and K dwarfs. Among 12,000 stars, 221 new variables were identified, including members of eclipsing and pulsating classes (see figure 1). The fraction of stars showing variability reaches 17% at $V = 14$, the bright (high photometric precision) end of the program's magnitude range. The fraction of stars that are variable peaks at colors both bluer and redder than the Sun. These features correspond to instability strip and late-type spotted stars respectively (see figure 2).

In the future Everett and Howell plan to perform multicolor time variability surveys to sample rich star fields, various galactic positions, and open and globular clusters. Their primary objective is to search for transits by extrasolar planets, but longer-time baselines and follow-up spectroscopy of interesting sources will provide a more complete census of variable sources within and external to the Galaxy.

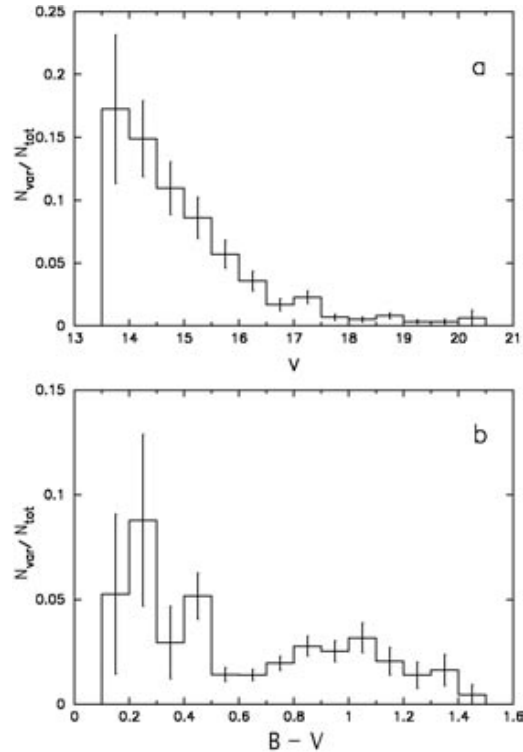


Figure 2. (a) The fraction of stars found to be variable as a function of V . The fraction is highest for the brightest stars since they are observed with the best precision. Approximately 17% of the brightest stars exhibit variations. (b) The fraction of stars found to be variable as a function of $B-V$. Pulsating stars in the instability strip account for most of the variability at blue colors ($B-V < 0.5$) while the fraction of variables among stars with Sun-like colors is relatively low. The variability fraction increases for colors redder than the Sun.



Imaging Polarimetry in the Ultraviolet

Jan Stenflo (ETH Zürich), Achim Gandorfer (ETH Zürich) & Christoph Keller (NSO)

Since 1994, a group from ETH Zürich, in collaboration with Christoph Keller, has carried out a series of observing runs at the McMath-Pierce facility with their polarimeter system ZIMPOL (Zürich Imaging Polarimeter). Since seeing and gain-table noise are eliminated with this system so that the polarimetric precision becomes limited only by photon statistics, noise levels as low as 5×10^{-6} have been achieved in combination with high spectral resolution. At this level of precision, *everything* in the solar spectrum is polarized, even in the absence of magnetic fields. In linear polarization, we see a spectrum that is as richly structured as the intensity spectrum, but which has a very different appearance, since the underlying physical processes are different. It is as if the Sun has presented us with an entirely new and unfamiliar spectrum, and we have to start all over to identify the spectral structures that we see. This new spectrum in linear polarization has therefore been called the “second solar spectrum.”

Since its first implementation, the ZIMPOL system has been continually upgraded, and new, more powerful versions have been put to use at NSO as they have become available. While the first generation (ZIMPOL I) could only image two of the four Stokes parameters simultaneously, the second generation (ZIMPOL II) had the capacity of imaging the full Stokes vector (by creating four simultaneous image planes on a single CCD detector chip). ZIMPOL I and II, however, could not be used for wavelengths below about 4500 Å. This was a serious limitation, since both the structural richness of the “second solar spectrum” and the polarization amplitudes increase greatly toward shorter wavelengths.

Therefore, during the last couple of years we have made a considerable investment to develop specially designed CCD sensors in collaboration with CCD manufacturer EEV. These sensors that have high efficiency throughout the UV, all the way down to the atmospheric cutoff near 3000 Å, while possessing an architecture that allows the fast (kHz range) ZIMPOL-type charge-shifting technology. To achieve high quantum efficiency in the UV, holes had to be etched in the polysilicon gate layer above the pixels, creating an Open Electrode Structuring (OES).

The new, UV-sensitive ZIMPOL system was used for the first time at NSO in an exploratory observing run in March 2002. The run exceeded our expectations, both in terms of system performance and in terms of the astounding richness of the polarized UV spectrum. It is like digging in a newly discovered “gold mine.” Here we can only provide a glimpse of what we observed.

Figure 1 shows the four Stokes vector images of the spectral region around the Ca I 4227 Å line, which has the strongest scattering polarization in the visible spectrum. The spectrograph slit has been placed 20 arcsec inside and parallel to the solar limb in a facular region. While the circular polarization (V/I) shows the familiar antisymmetric signatures of the longitudinal Zeeman effect, the linear polarization in the Ca I line is due to scattering polarization (while the transverse Zeeman effect shows up in many of the blend lines). The strong variations along the spectrograph

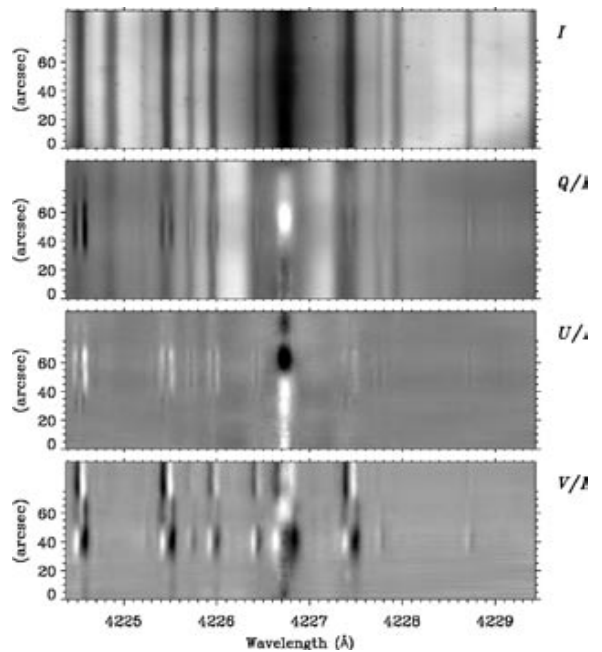


Figure 1. Stokes vector image of the spectral region around the Ca I 4227 Å line. The recording was made in a facular region 20 arcsec inside the limb.

slit of the linear (Q/I and U/I) polarization in the Ca I line core are due to the Hanle effect from the spatially structured chromospheric magnetic fields. The Hanle effect is a new tool to diagnose aspects of solar magnetic fields that cannot be seen with the Zeeman effect. The ambiguities that often occur in the interpretation of the Hanle signatures can be removed by using combinations of spectral lines with different sensitivities to the Hanle effect. Since the UV presents us with a much greater selection of such lines than other spectral regions, the UV range is of unique importance for the application of Hanle diagnostics.

continued



Imaging Polarimetry in UV continued

Figure 2 gives another example of what the UV region has to offer. The recording was made with the spectrograph slit positioned 6 arcsec inside and parallel to the solar limb at the heliographic south pole, covering the wavelength range around the Be II resonance doublet at 3130.414 and 3131.058 Å. Since the recording was made in a very quiet region, the scattering polarization did not show spatial structuring, so we could average the 2-D spectra along the spectrograph slit to produce the 1-D spectra in figure 2. At these UV wavelengths the continuum is strongly polarized, and the majority of the lines suppress (depolarize) the continuum. In contrast, the left Be II line exhibits a strong, positive (electric vector parallel to the limb) polarization peak, while the right Be II line depolarizes the continuum.

The two Be II lines are due to transitions with a quantum-number structure, including hyperfine-structure splitting, that is identical to the well-known Na I D₂ and D₁ lines at 5889.97 and 5895.94 Å, which have polarization signatures that remain enigmatic. Using the notation D₂ and D₁ in figure 2, the general quantum-mechanical expectation is that the D₂ line should be polarized, while the D₁ line should be unpolarized. Though various diagnostic applications of such observations are possible (determination of beryllium abundance, radiative transfer physics, Hanle diagnostics),

the focus of these initial, exploratory observations is to identify the multitude of phenomena in the second solar spectrum and to clarify the underlying physics.

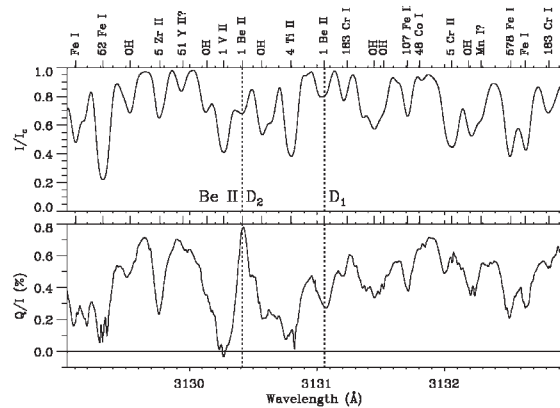


Figure 2. The spectrum in intensity (top panel) and degree of linear polarization (bottom panel) in the spectral region around the Be II D₂ (3130.414 Å) and D₁ (3131.058 Å) lines. The recording was made in a quiet region at the heliographic south pole, 6 arcsec inside the limb. The vertical dotted lines mark the resonant wavelengths of the two beryllium lines.

Imaging Polarimetry of Jupiter and Saturn with ZIMPOL

Daniel Gisler & Hans Martin Schmid (ETH, Zürich)

In March 2002, we obtained imaging polarimetry of the planets and bright stars using the Zürich Imaging Polarimeter (ZIMPOL) at the 1.5-m McMath-Pierce telescope. J. Stenflo, A. Gandorfer, and C. Keller observed the Sun with spectropolarimetry during the day (see previous article in this *Newsletter*) and we observed at night. Our aim for these test measurements was to gain experience with this type of instrument for stellar (nighttime) applications.

The ZIMPOL technique is based on a fast, electro-optical polarization modulator working in the kHz range, in combination with a special CCD camera performing on-chip demodulation of the signal. ZIMPOL has been used very successfully for polarimetric measurements of the Sun. In fact, the polarimetric accuracy was improved by about two orders of magnitude in S/N. Accordingly, we have adapted the ZIMPOL technique for nighttime astronomy in order to exploit its unprecedented measuring accuracy.

Our first tests at Kitt Peak used a ferro-electric liquid crystal (FLC) retarder plate—where the optical axis can be switched by 45°—as a polarization modulator. The FLC allows lower

modulation rates of 1 kHz, instead of the 40-kHz rates of piezo-elastic modulators. Thus, the FLC enables longer integration times of up to 40 seconds. This is because the CCD demodulation shifts are limited to about 10⁵ modulation cycles due to anomalous charge transfer effects in the CCD. The slower modulation also reduces CCD heating. In our case, the thermoelectric cooling achieved a lower temperature of -30°C, instead of the norm of -10°C. This FLC modulator was combined with “spare parts” from the solar ZIMPOL instrument for the observing run.

Our tests with the McMath-Pierce telescope are very promising. For Jupiter and Saturn, high-quality maps for the linear polarization in four narrowband filters centered at 4500 Å, 5500 Å, 6000 Å, and 7300 Å, with a width of 200 Å, were obtained. The figure shows the reflected sunlight from Jupiter and Saturn at 5500 Å. The other maps are qualitatively the same except for some small but significant color trends. Both planets have a low polarization at the disk center, because the scattering angle is close to 180° (backscattering), as is always

continued

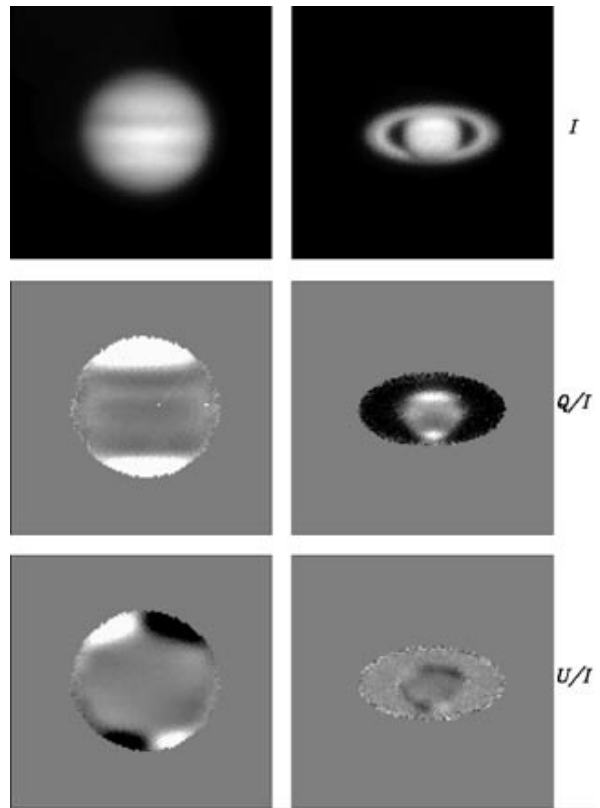


Imaging Polarimetry continued

the case for the outer planets observed from Earth. Both objects exhibit a limb polarization perpendicular to the limb that is much stronger at the poles than at the equator.

The perpendicular limb polarization is caused by a well-known second-order scattering effect. Photons reflected after one scattering in the planet atmosphere are practically nonpolarized, because the scattering angle is close to 180°. After the first scattering, photons travel predominantly parallel to the planet surface before being reflected toward us by the second scattering process. Because the polarization angle induced in a scattering is perpendicular to the propagation direction of the incoming photon, a polarization perpendicular to the limb results. The polarization at the poles is much higher because the Rayleigh scattering atmosphere is deeper, or the effective cloud level is lower than in the warmer equatorial regions. In the rings of Saturn, practically no polarization structure is seen as should be expected from a mixture of reflecting solid debris bodies.

Much has been learned from this observing run and we are confident that the ZIMPOL technique has a huge potential for astrophysical polarimetry. However, further improvements are required, such as lower CCD dark-current and read-out noise levels with an improved cooling system, or the development of an achromatic modulator system for broadband imaging polarimetry. This effort is warranted since the new 8–10-m telescopes provide sufficient light-collecting power to obtain a very high polarimetric accuracy for bright objects. For example, a spectropolarimetric accuracy of $\Delta = 10^{-4}$ with a spectral resolution of 300 can be achieved for a 9th-magnitude object with an integration time of one hour. For broadband imaging, this polarimetric accuracy is possible for a 13th-magnitude object. Such an improvement in measuring accuracy will open up many new opportunities for investigations of stellar magnetic fields, or scattering gas and dust structures near stars and active galactic nuclei.



Images of the intensity I and Stokes parameters Q/I and U/I for Jupiter and Saturn at 5500 Å. The images are not completely corrected for the telescope polarization. The polarization, however, is displayed relative to the polarization at the center of the planet disk, which is set to zero (the intrinsic polarization is very small). The gray scale in the Stokes polarization images goes from -1% (black) to +1% (white). The maximum polarization at the poles of Jupiter is greater than +5%.

12- μm Magnetometry with Visible Tip-Tilt Image Stabilization

George McCabe, Don Jennings, Drake Deming (NASA GSFC) & Christoph Keller, Claude Plymate (NSO)

In April 2002, the Celeste spectrometer was used with the McMath-Pierce tip-tilt image stabilizer, operating in the visible, to test whether this technique would improve measurements of solar magnetic fields in the thermal IR. Combined with a computer-controlled wave-plate polarization analyzer and synchronized telescope guider stages, Celeste creates high-resolution IR (12.32- μm) maps

of active regions in all four Stokes parameters. The Celeste detector array double-samples the diffraction-limited spot of the telescope, but the effective limit on the spatial resolution of spectral-image scans is set by atmospheric motion and telescope tracking errors. We were able to demonstrate that the tip-tilt system, operating in the visible, successfully eliminates the unwanted motion in the IR image.

continued



12- μm Magnetometry continued

Short integration time measurements of the solar limb recorded with and without the tip-tilt mirror activated show how image motion is removed in the IR using 1-D. Figure 1 compares limb profiles for 10 scans (each 1/10 sec). Note that the dip in the curve near the middle is the extension of the Mg I emission line beyond the solar limb. In the left frame, the spread in the data due to limb motion in the nonstabilized case is approximately 3 arcsec. Thus, without stabilization, a time average of the measurements is degraded by a significant smearing of the limb. In the right frame, the limb motion during stabilization is reduced to less than 1 arcsec.

Measurements of Stokes parameters in a sunspot were made to compare closed-loop and open-loop tip-tilt operation. Limb guiders were not used, so as to avoid any contribution of the telescope control system beyond tracking errors, which accumulate slowly on the scale of the data read times. Manual guide corrections were made between closed-loop integrations to compensate for telescope drift, and to maintain the position of the image near the center of the range of travel (20 arcsec) of the tip-tilt mirror. In figure 2, the plot of Stokes V shows the difference in appearance of the spectral profiles for the closed-loop and the open-loop cases. A larger separation of σ components is distinctly seen in the darker curve (closed-loop), as compared with the lighter curve (open-loop). Also, the line-of-sight magnitude of B is larger in the data with tip-tilt turned on. Since the average slit position on the spot is biased in the direction of telescope drift, we can't yet say for sure whether these differences are completely due to image stabilization, i.e., they may be partly due to looking at different places in the spot. However, it is clear from the data that the tip-tilt

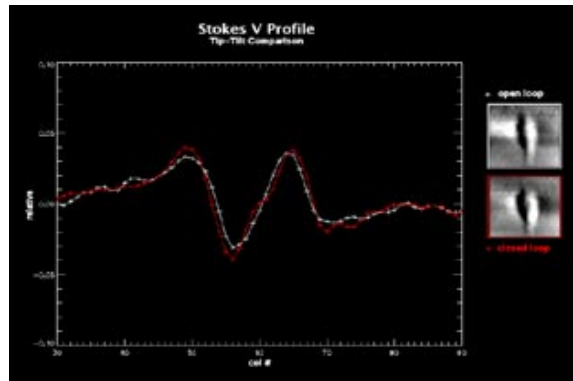


Figure 2

system is providing improved image stability at 12 μm . We anticipate that use of the tip-tilt correction will produce higher precision in magnetic field maps. The full potential of this improvement in the IR will be realized with the Advanced Technology Solar Telescope (ATST) and its planned adaptive optics facility. We anticipate developing this technique further in upcoming runs at the McMath-Pierce telescope.

The Celeste instrument system was built by the NASA Goddard Space Flight Center (G. McCabe, D. Jennings, D. Deming). Our work is supported in part by the NASA Solar Physics Program. The adaptive optics image stabilizer was developed at the National Solar Observatory by C. Keller and C. Plymate.

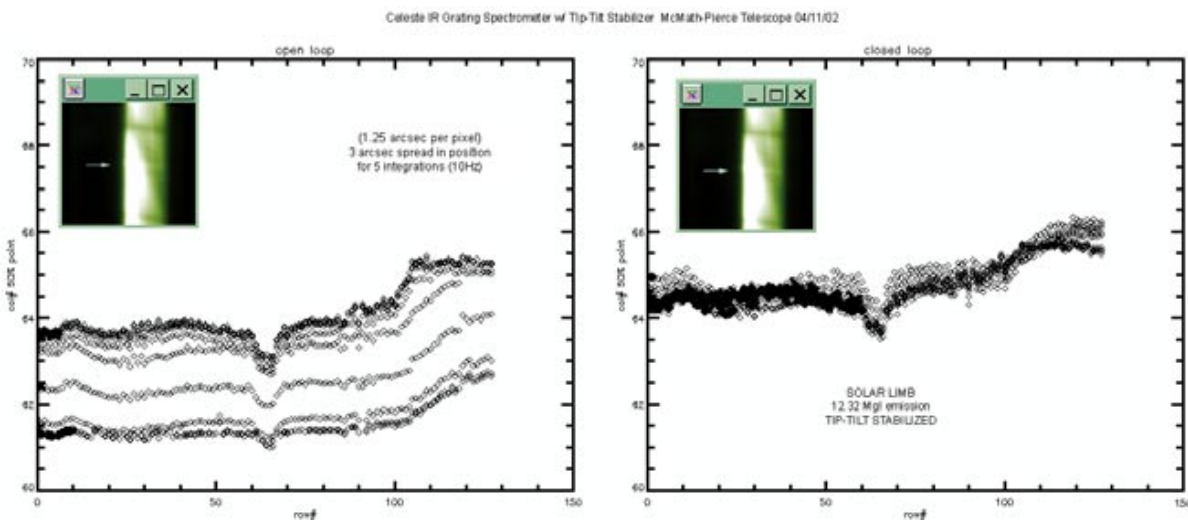


Figure 1